Optimal Graph-Based Segmentation of 3D Pulmonary Airway and Vascular Trees Across Bifurcations*

Xiaomin Liu[1], Danny Z. Chen[1], Xiaodong Wu[2], and Milan Sonka[2]

[1] Department of Computer Science & Engineering, University of Notre Dame, xliu9@nd.edu
[2] Department of Electrical & Computer Engineering and Department of Radiation Oncology, The University of Iowa

Abstract. Segmenting airway and vascular trees in CT volume images plays a fundamental role in pulmonary image analysis. However, accurate assessment of complete tree morphology is difficult due to their complex nature. In this paper, we extend an optimal graph search based technique to identifying tree-structured airways and lung vessels with one or more interrelated surfaces. Based on a pre-segmentation that preserves the object topologies, our approach utilizes the 3D medial axes to resample the volume image and construct a geometric graph. By designing appropriate cost functions, the segmentation of both airways and vessels is performed across tree bifurcations in a single optimization process for the entire tree. Segmentation results of double surfaces for airways and single surface for vascular trees are presented.

1 Introduction

The airway and blood vessels are two major components of the human lung. Quantitative assessment of both the airway and vascular trees provides important information for functional understanding of pulmonary anatomy and objective measures of lung diseases. Due to the large image sizes and highly branching structure, it is tedious and time-consuming to manually locate individual tree branches and draw their contours on 2D slices. Furthermore, 2D manual tracing and image analysis methods may not be as effective and reliable, since they lack the ability to incorporate 3D information. Hence, developing automated and accurate 3D segmentation methods for lung images is a critical task in pulmonary image analysis and computer aided diagnosis. Further, airway trees and vessel trees may have multiple interrelated layers of surfaces for segmentation, some of which are extremely hard to detect individually. Several techniques have been proposed to segment the tubular lung objects ([1, 2]), but they cannot guarantee global optimality.

* This research was supported in part by NSF Grant CCF-0515203 and NIH NIBIB Grant R01-EB004640-01A2.

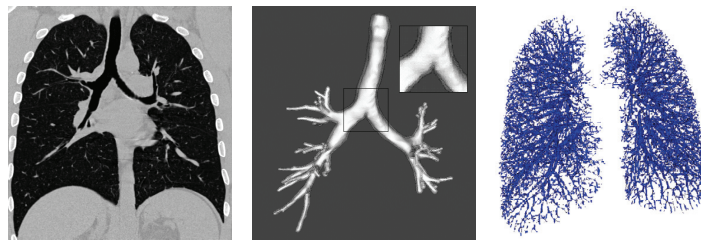

(a) (b) (c)

Fig. 1. Illustrating 3D airway and vessel segmentation: (a) The original lung CT image; (b) the rendered airway inner and outer walls with cross bifurcation segmentation; (c) the rendered vascular tree.

Wu and Chen [3] reported an optimal graph search based algorithm, which was extended to multiple surface segmentation by Li *et al.* [4]. These graph search based schemes transform the image segmentation problem to computing a minimum-cost closed set in a derived vertex-weighted graph, and obtain optimal segmentation. The methods have been successfully applied to non-branching airway segmentation [4] and MR arterial wall segmentation [4], but it did not directly extend to segmenting objects with a tubular and tree-like topology such as airways or blood vessels (see Fig. 1). The methods in [3, 4] are only suitable for the objects that have a relatively simple topology (e.g., cylindrical or spherical). In these cases, a 3D geometric graph can be built either by unfolding the sought surfaces to terrain-like surfaces or resampling the image along the normal surface directions within a narrow band. However, these "simple" methods for building 3D graphs are not directly applicable to objects with complicated structures since they may cause severe interferences among the resampled vectors and may fail to intersect (or capture) the sought surfaces.

In this paper, we present a technique for segmenting multiple interrelated layers of surfaces for airway and vessel trees. Specifically, to address the above-mentioned drawbacks, we propose a new scheme for building the 3D graphs for segmenting tubular and tree-structured objects. To overcome the difficulty of segmenting branching structures, we use medial axes and surface dilation to guide and produce an effective image resampling. Our graph search on the resampled images uses task-specific cost functions for airway and vascular trees. Consequently, we obtain segmentation results of multiple interrelated layers of surfaces for airway and vessel trees with significantly improved quality.

2 Method

The graph search based algorithms [3, 4] solve the segmentation problem by transforming it to finding a minimum-cost closed set in a directed vertex-weighted

graph, which is solvable in polynomial time. Our graph search based image segmentation approach consists of the following four major steps:

(1) Pre-segmentation. A pre-segmentation is needed to provide the basic information about the object's global structure. It is not necessary for the pre-segmentation to be locally accurate. However, it is crucial to preserve the topology of the target object. If the pre-segmentation does not yield a mesh, we also need to transform the volumetric result into a mesh representation.
(2) Image resampling. Based on the outcome of the pre-segmentation, the image is resampled on each vertex of the initial surface mesh, resulting in a set of vectors (called *columns*) of voxels. In this paper, the medial axes are applied to determine the directions and lengths of the resampling columns.
(3) Graph construction. Each voxel in the columns is considered as a node in the graph. There are three types of edges, representing the relations of voxels within the same surface or between different surfaces. A cost is assigned to each node which reflects the certain property of the sought surfaces.
(4) Graph search. Finally, we apply a minimum s-t cut algorithm [3, 4] to the resulting graph to simultaneously search for multiple interrelated surfaces.

For segmenting tubular and tree-structured objects, the most nontrivial task is to build a vertex-weighted geometric graph to model the volumetric image. When constructing this graph model, we need to carefully resample the volumetric image so that the following two constraints are satisfied: 1) All the sought surfaces must be captured by the graph; 2) the relations among the voxel columns should be consistent with the surface topology specified by the preliminary mesh from the pre-segmentation, meaning that interferences among different voxel columns cannot be allowed (more on this later).

2.1 Pre-segmentation

The algorithm we use for the pre-segmentation of pulmonary vascular trees is based on a hybrid method of the tube enhancement filtering and traversal approaches [5]. First, the tube enhancement based on the cylindrical shape model using an eigenvalue of the Hessian matrix serves as a filter to extract vessels. Then, a traversal step detects the change of signs of those eigenvalues to improve the vessel's connectivity. Finally, objects with many branch points are selected to distinguish between vascular trees and noise components. Airway trees are pre-segmented using commercially available Pulmonary Workstation PW+ software (VIDA Diagnostics, Oakdale, IA). Once a labeled image is generated by the pre-segmentation, it is transformed into a triangulated mesh using the marching cube algorithm.

2.2 Image resampling based on medial axes

To segment an optimal surface in the image using the corresponding preliminary meshed surface, our approach needs to perform a resampling of the image for

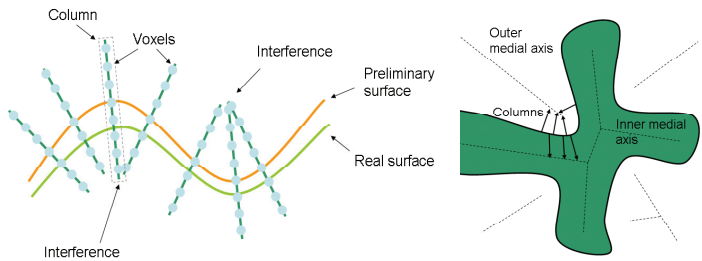

Fig. 2. Illustrating the image resampling: (a) The interferences caused by inappropriate column lengths, (b) a 2D example of image resampling based on medial axes.

every surface vertex along the normal direction of the meshed surface at that vertex, resulting in a column of voxels for each vertex. In this process, we seek to avoid two "bad" situations: (1) The length of a column is too long, so that it interferes with (intersects) other columns; (2) the length of a column is too short, so that it fails to capture enough information about the real surface. To avoid possible interferences among the resampled columns, we need to determine the proper directions and lengths for the columns. Intuitively, the normal direction at each mesh vertex is the direction without any bias or prior information about the location of the real surface.

A medial axis of the preliminary surface is a set of points each of which has at least two nearest points on the surface [6]. At each mesh vertex, the medial axis determines the maximum distance that a column can be extended along the normal direction without any interference with other columns. Although the exact computation of the medial axis is possible in principle, it is complicated to implement due to significant algebraic difficulties [6] – approximate solution can be obtained using computational geometry. Suppose the vertices of the mesh form a point set S. We can compute the Voronoi diagram and the dual Delaunay triangulation of S in 3D [7]. The medial axis is computed by using the poles in the Delaunay triangulation, which are selected from the centers of the big Delaunay balls adjacent to vertices. Then we assign a pole to each of the mesh vertices by selecting the largest pole among the vertex's k-nearest neighbors, in order to reduce the impact of possible noise on the surface [7]. Next, the lengths of the columns are obtained by computing the distances from the mesh vertices to their corresponding medial axis points (on both the inner and outer medial axes of the preliminary surface, Fig. 2).

A sought surface may contain very sharp angles at its branches. In such situations, a medial axis could be very close to the branching portions of the surface and consequently the columns computed based on the medial axis could

be quite short, giving very little flexibility to the graph search algorithm. To avoid this problem, we first grow (dilate) the preliminary surface by a certain distance, and then compute the columns based on the grown surface and its medial axes. The distance we used in the experiments is 3 voxels, which should be depending on the size of the object. With an appropriate value for the growth distance, we can obtain a set of columns that extend across the sought surfaces.

2.3 Graph search based segmentation

A graph $G = (V, E)$ has a set V of nodes (or vertices) that are connected by edges in E. In this paper, the nodes in V of G are voxels in the resampled volumetric image, which are organized by the columns. Each column of nodes is associated with a vertex of the preliminary mesh, and is sampled along the normal direction at that vertex. We assign edges to connect neighboring nodes in G and to ensure the geometric constraints (e.g., the *smoothness constraint* and the *separation constraints* of the surfaces [4]). Generally, the graph G is constructed in a similar manner as in [4].

Airway tree segmentation The detection of airway outer wall is difficult since the outer surface is often surrounded by other adjacent tissue with similar gray scale intensities in CT images. Instead of segmenting the airways section by section and gluing the branches together afterwards, we consider the airway tree as a whole and search for both the optimal inner and outer walls simultaneously.

For each sought surface, we construct a graph that is designed to contain that surface. At each mesh vertex v, there are two columns, corresponding to the inner and outer surfaces, respectively. Denote these two columns at vertex v by $Col_i(v) = \{n_i(v, 0), \ldots, n_i(v, K-1)\}$ and $Col_o(v) = \{n_o(v, 0), \ldots, n_o(v, K-1)\}$. Within every column, say, $Col_i(v)$, each node $n_i(v, k)$ is connected by a directed edge to $n_i(v, k-1)$ for $k \geq 1$. Between each pair of adjacent columns, a set of edges is assigned to ensure the *smoothness constraint* [4] within the surface. Let v_1 and v_2 be two adjacent vertices on the mesh, and suppose $n_i(v_1, k_1)$ is connected to $n_i(v_2, k_2)$ by an inter-column edge. Then the smoothness constraint Δ enforces that:

$$-\Delta \leq k_1 - k_2 \leq \Delta \tag{1}$$

With the smoothness constraint, we avoid any dramatic change of the neighboring voxels on the same surface, which consequently results in smooth surfaces of the sought medical objects. In the case of double surface detection, another set of edges, called inter-surface edges, is added to impose the *surface separation constraint* [4] between the two surfaces. The inter-surface edges are assigned between vertices $n_i(v, k_i)$ and $n_o(v, k_o)$ for all $v \in V$ so that the following separation constraint is satisfied:

$$\delta^l \leq k_i - k_o \leq \delta^u \tag{2}$$

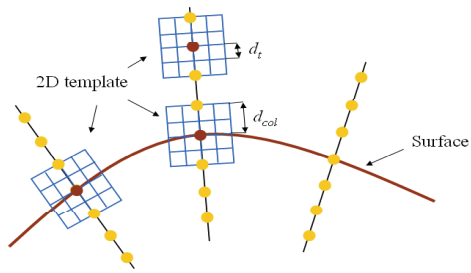

Fig. 3. Illustrating the cost function constructed at each node of the graph.

where δ^l (resp., δ^u) specifies the smallest (resp., largest) allowed distance between the two sought surfaces. (Assume that $\delta^l, \delta^u > 0$.) The separation constraint ensures that two sought surfaces are not too far away and also not too close to each other (e.g., they may not be allowed to intersect).

After the graph is constructed with the above three types of edges between the nodes in the columns, we need to assign a cost function to each of these nodes. The cost function must reflect the possibility for a voxel (node) to belong to a certain surface. For airway wall detection, the two surfaces differ from each other in the direction of intensity change. Since the airway lumen is darker than the airway wall, the intensity increases from low to high at the inner border. Conversely, the intensity decreases from high to low at the outer border when only parenchymal tissue is adjacent. However, this intensity change for the outer border shall also hold when non-parenchymal surrounding tissue is present. Since the airway wall is not completely connected to the surrounding tissue, there ought to be a little gap outside the wall that represents a "lower" intensity.

The cost function we use for airway segmentation is a combination of the first and second derivative edge detectors and is based on the cost function proposed in [8]. This is due to the property that the two edge detectors tend to yield the maximum magnitude on one or the other side of the true edge, causing certain over-estimate or under-estimate of the airway wall position. Thus, a weighted sum of the first and second derivatives works better for the accurate border location. Ideally, a 3D edge detector should be applied in our situation because of the 3D nature of the image. However, a test of these two edge detectors shows that the 3D edge detector performs similarly as the 2D one but with a significant increase of the computational overhead. In order to achieve a higher efficiency, the 2D edge detector is adopted to build the cost function at each node v

$$Cost_{outer}(v) = \omega \cdot I_t(v) * M_{Sobel_1} + (1-\omega) \cdot I_t(v) * M_{Marr} \tag{3}$$

$$Cost_{inner}(v) = \omega \cdot I_t(v) * M_{Sobel_2} + (1-\omega) \cdot I_t(v) * M_{Marr} \tag{4}$$

where M_{Sobel_1} and M_{Sobel_2} represent two inversely oriented 2D Sobel templates, and M_{Marr} represents the 2D Marr template (all in 5×5 size). $I_t(v)$ is a 5×5 gray-scale image template resampled from the 3D image around the node v. As we did for the resampling of columns, the template is also sampled along the corresponding vertex's normal direction (as illustrated in Fig. 3). Thus, the 2D image template is centered at the node v and is on a plane perpendicular to the surface. The voxels are sampled at the interval size d_t such that

$$d_t = d_{col}/2 \tag{5}$$

where d_{col} is the interval between neighboring voxels in a resampled column.

Vascular trees segmentation For the vascular tree segmentation, the graph is constructed in the similar manner although there is only one surface to be detected (the only one visible on CT image). Hence, only the intra-column and inter-column edges are needed to build the graph. The cost function used for vascular tree segmentation is the magnitude of gradient computed from the Gaussian smoothed images.

3 Validation of Pulmonary Image Segmentation

The validation of airway and vascular tree segmentation has been performed on a set of 6 CT scans of lung CT images. The sizes of the images vary from $512 \times 512 \times 562$ to $512 \times 512 \times 671$, voxel size $0.68 \times 0.68 \times 0.6\text{mm}^3$, Siemens Sensation 64-slice MDCT. After an initial surface of the airway inner wall is extracted (Section 2.1), our graph search approach succeeded in extracting the outer wall as well as optimizing the location of the inner wall in all 6 cases. An example of the cross bifurcation segmentation is shown in Fig. 4. To segment the vascular trees, each connected blood vessel component is filtered out and labeled with a different number. In comparison with the pre-segmentation results (which were considered final till now), the graph search captures the wall surfaces more accurately especially across bifurcations. (See Fig. 5.) While the initial results show the approach is promising for simultaneously segmenting single- and multiple-surfaces of pulmonary airway and vascular trees, we understand that more quantitative evaluation needs to be done in our following work.

4 Discussion and conclusion

In this paper, we extended the optimal graph search based approaches introduced in [3, 4] to segmenting airway and vascular trees in 3D pulmonary CT images. By using medial axes to guide the resampling, the 3D image is sampled properly based on the preliminary segmentation. Even though both the airways and vessels have complicated tree structures (airways with multiple interrelated surfaces), our proposed resampling scheme is able to extract sufficient information from the image data and provide it to the graph search algorithm to identify the

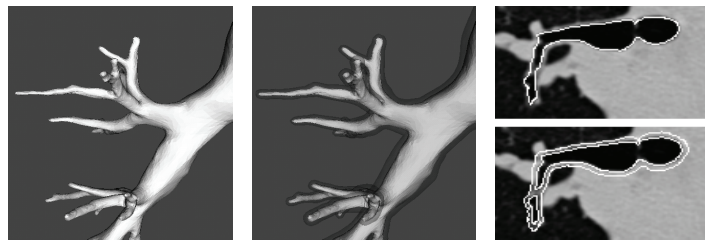

(a) (b) (c)

Fig. 4. Airway segmentation: (a) The inner wall (result of pre-segmentation); (b) double surfaces after graph search; (c) the comparison of preliminary result and graph search result in 2D slices. Note that the inner as well as outer surfaces are smooth and three-dimensionally accurate across the airway branching.

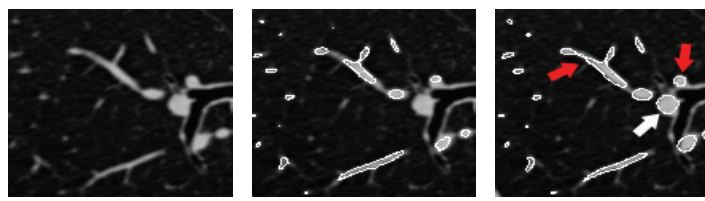

(a) (b) (c)

Fig. 5. Vascular tree segmentation results: (a) The original image; (b) the pre-segmentation; (c) the graph search result showing improved delineation (red arrows). Note the ability to correctly detect the surface even if the preliminary segmentation fails locally – as long as the preliminary segmentation is in the vicinity of the desired surface (white arrow).

optimal surfaces. By applying cost functions with directional information, our algorithm succeeds in detecting both the inner and outer surfaces of the airway walls as well as the vascular wall surfaces across bifurcations. As shown by the examples, the segmentation considerably improved the results of the preliminary segmentation.

References

1. Aykac, D., Hoffman, E.A., McLennan, G., Reinhardt, J.M.: Segmentation and analysis of the human airway tree from three-dimensional X-ray CT images. IEEE Trans. Med. Imag. **22** (2003) 940–950

2. Boldak, C., Rolland, Y., Toumoulin, C.: An improved model-based vessel tracking algorithm with application to computed tomography angiography. Journal of Biocybernetics and Biomedical Engineering **23** (2003) 41–63
3. Wu, X., Chen, D.Z.: Optimal net surface problems with applications. In: Widmayer, P., Triguero, F., Morales, R., Hennessy, M., Eidenbenz, S., Conejo, R. (eds.) ICALP 2002. LNCS. (2002) 1029–1042
4. Li, K., Wu, X., Chen, D.Z., Sonka, M.: Optimal surface segmentation in volumetric images - A graph-theoretic approach. IEEE Transactions on Pattern Analysis and Machine Intelligence **28** (2006) 119–134
5. Shikata, H., Hoffman, E.A., Sonka, M.: Automated segmentation of pulmonary vascular tree from 3D CT images. In Amini, A.A., Manduca, A., eds.: Proc. of SPIE Medical Imaging 2004: Physiology, Function, and Structure from Medical Images. Volume 5369. (2004) 107–116
6. Attali, D., Boissonnat, J.D., Edelsbrunner, H.: Stability and computation of medial axes: A state of the art report. In T. Möller, B.H., Russell, B., eds.: Mathematical Foundations of Scientific Visualization, Computer Graphics, and Massive Data Exploration. Springer-Verlag, Mathematics and Visualization (2007)
7. Dey, T.K., Sun, J.: Normal and feature estimations from noisy point clouds. Technical Report OSU-CISRC-7/50-TR50 (2005)
8. Sonka, M., Reddy, G.K., Winniford, M.D., Collins, S.M.: Adaptive approach to accurate analysis of small-diameter vessels in cineangiograms. IEEE Trans. Med. Imag. **16** (1997) 87–95